Tunable Plasma Linearizer for Compensation of Nonlinear Energy Chirp

Yipeng Wu, Jianfei Hua, Zheng Zhou, Jie Zhang, Shuang Liu, Bo Peng, Yu Fang, Xiaonan Ning, Zan Nie, Qili Tian, Chih-Hao Pai, Yingchao Du, Wei Lu, Warren B. Mori, and Chan Joshi

Phys. Rev. Applied **16**, 024056 — Published 30 August 2021

DOI: 10.1103/PhysRevApplied.16.024056

Tunable Plasma Linearizer for Nonlinear Energy Chirp Compensation

Yipeng Wu,[1,2] Jianfei Hua,[1,*] Zheng Zhou,[1,†] Jie Zhang,[1] Shuang Liu,[1] Bo Peng,[1] Yu Fang,[1] Xiaonan Ning,[1] Zan Nie,[1,2] Qili Tian,[1] Chih-Hao Pai,[1] Yingchao Du,[1] Wei Lu,[1,‡] Warren B. Mori,[2] and Chan Joshi[2]

[1]*Department of Engineering Physics, Tsinghua University, Beijing 100084, China*

[2]*University of California, Los Angeles, California 90095, USA*

Removal of undesired nonlinear time-energy correlation (energy chirp) present in the relativistic electron beams is crucial for many accelerator-based scientific applications, such as free-electron laser, high-energy electron radiography and MeV ultrafast electron microscopy. Here we propose and demonstrate that a low-density plasma section can be used as a passive "linearizer" to significantly compensate for the nonlinear energy chirp imprinted on the beam by the curvature of the radio-frequency field in a conventional accelerator. Physically, the passage of the beam through the plasma excites a strong quasi-cosinoidal longitudinal decelerating wakefield that acts to mitigate the beam nonlinear energy chirp by superimposing a reverse chirp on the beam. Time-resolved phase space measurements, combined with high-fidelity three-dimensional particle-in-cell simulations show that the longitudinal phase space of the beam core is almost completely linearized, leading to a fourfold reduction of the beam overall energy spread from 1.48‰ to 0.36‰ (FWHM).

I. INTRODUCTION

Many forefront accelerator-based applications, such as free-electron laser (FEL) [1–4], high-energy electron radiography (HEER) [5, 6] and MeV ultrafast electron microscopy (MeV-UEM) [7–9] are revolutionizing science at ultrafast and ultra-small scales. For these applications, a precise control of the electron beam longitudinal phase space (LPS) - namely a constant energy along the longitudinal dimension - is critical. However, since the beam is normally generated and accelerated in a linac powered by radio-frequency (RF) waves, nonlinear energy chirp will be induced on the beam LPS due to the cosinoidal RF time-curvature. This nonlinear energy chirp is usually detrimental to the application performance. In FELs, the nonlinear energy chirp causes deterioration of the bunch compression and degradation of the FEL bandwidth. In HEER and MeV-UEM facilities, the nonlinear energy chirp leads to beam energy spread increase and thus serious chromatic aberrations growth, which may significantly reduce spatial resolutions. Therefore, removal of such nonlinear time-energy correlation or linearization of the beam LPS is highly desirable for improving the performance of these scientific machines.

Typically, the correction of the nonlinear energy chirp can be accomplished using a high harmonic cavity [10, 11]. However, this active compensation method requires an extra expensive RF station, as well as precise control of the amplitudes and phases of the RF wave within the structures. Besides, the beam energy will be reduced by a relatively large fraction. The beam LPS can also be linearized by shaping the photoinjector laser pulse [12]. However, this method may increase the beam emittance and requires magnetic compressors, which may be not suitable for MeV-UEM application. Another LPS linearization method is to exploit the interaction of the beam and its self-induced longitudinal wakefield in RF sections [13] or passive devices such as dielectric-lined and corrugated metallic structures [14–17]. However, for this method, the beam should be accurately kept very close to the structure axis. Otherwise, dipole wakefields can be induced, leading to emittance growth and even beam breakup instability. In addition, the planar structure geometry also excites time-dependent quadrupole wakefields that can increase beam emittance even for an on-axis beam.

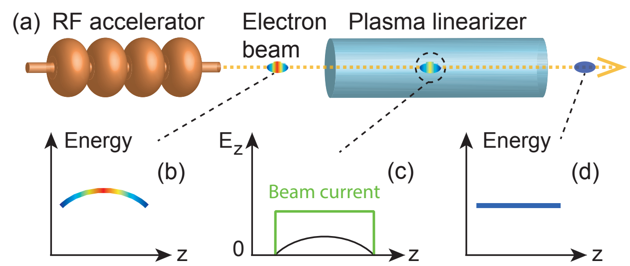

FIG. 1. (a) Schematic diagram of the plasma linearizer. (b) The initial LPS. (c) The beam current profile (green line) and the on-axis longitudinal wakefield E_z excited by the beam in the plasma linearizer (black line). (d) The final LPS.

An alternative, RF-free approach to correct the undesired energy correlation in the electron beam is to utilize a plasma. Recently, plasma-based dechirpers have been proposed and demonstrated [18–22], which focus on removing beam linear energy chirps. Here, we propose and experimentally demonstrate that a tunable plasma section can also serve as a linearizer that can remove beam *nonlinear energy chirps*. In this scheme [Fig. 1(a)], an electron beam with a nonlinear energy chirp [Fig. 1(b)] is sent through a separate low-density plasma column to excite a strong quasi-cosinoidal longitudinal wakefield [Fig. 1(c)]. By properly choosing the wavelength of the wakefield, the nonlinear energy chirp can be effectively cancelled during the propagation [Fig. 1(d)]. The net linearizing effect can be easily tuned by changing the density and length of the plasma. Apart from being cheaper and less complex than using RF harmonic cavities, this passive compensation scheme greatly decreases the beam energy reduction factor and can be widely applicable to all FEL, HEER and MeV-UEM facilities. Moreover, the field strength in a plasma is much larger than that in dielectric-lined or corrugated metallic structures for similar beams, thus making the linearizer device more compact.

II. THEORETICAL ANALYSIS

To quantify the effectiveness of a plasma linearizer, a theoretical analysis has been carried out using both linear and nonlinear theories [23–25]. We begin by initializing a uniform plasma with density of n_p and an electron beam with density profile of $\rho_b(r,\xi) = n_b\sigma(r)f(\xi)$, where n_b is the beam peak density, $\sigma(r)$ is the normalized transverse profile, $f(\xi)$ is the normalized longitudinal profile and $\xi = ct - z$ represents the longitudinal position relative to the beam.

For an underdense beam ($n_b < n_p$), linear plasma wakes are excited and the longitudinal wakefield E_z is

$$\frac{E_z(r,\xi)}{E_p} = R(r)Z(\xi) \tag{1}$$

where

$$R(r) = k_p^2 \int_0^\infty r'dr'\sigma(r')I_0(k_p r_<)K_0(k_p r_>) \tag{2}$$

$$Z(\xi) = \frac{n_b}{n_p}k_p \int_{-\infty}^{\xi} d\xi' f(\xi')\cos k_p(\xi - \xi') \tag{3}$$

Here $k_p = \sqrt{n_p e^2/m\varepsilon_0 c^2}$ is the inverse plasma skindepth and $E_p = mk_pc^2/e$ is the wave-breaking field. I_n and K_n are the modified Bessel functions of order n, and $r_<$ and $r_>$ respectively denote the minimum and maximum of r and r'.

For simplicity, we consider beams with transverse Gaussian [$\sigma(r) = \mathrm{e}^{-r^2/2\sigma_r^2}$, where σ_r is the spot size] and longitudinal flat-top [$f(\xi) = 1$ for $-L_b/2 \le \xi \le L_b/2$, where L_b is the full bunch length] profiles. In the narrow beam limit ($k_p\sigma_r \ll 1$), $R(r)$ within the beam has a weak dependence on r and can be expanded asymptotically as $R(r) \approx R(0) \approx -k_p^2\sigma_r^2\ln(k_p\sigma_r)$. Therefore E_z within the beam can be approximated as its on-axis value, given by

$$\frac{E_z(r,\xi)}{E_p} \approx \frac{E_z(0,\xi)}{E_p} \approx -\ln(k_p\sigma_r)\frac{2I_b}{I_A}\cos(k_p\xi + \frac{k_pL_b}{2} - \frac{\pi}{2}) \tag{4}$$

where I_b is the beam peak current and $I_A \approx 17$ kA is the Alfven current. We have calculated E_z fields produced by a 370-pC electron bunch with $n_b = 1.9\times10^{13}$ cm^{-3}, $\sigma_r = 80$ μm and $L_b = 3$ mm (10 ps) in three different plasma densities [$n_p = 2.1\times10^{13}$ cm^{-3} ($k_pL_b = 2.6$), $n_p = 3.1\times10^{13}$ cm^{-3} ($k_pL_b = \pi$) and $n_p = 4.1\times10^{13}$ cm^{-3} ($k_pL_b = 3.6$)]. They are shown in Fig. 2(a) with dashed lines, which are in good agreement with the simulation results [solid lines in Fig. 2(a)] obtained using the full three-dimensional (3D) particle-in-cell (PIC) code QuickPIC [26–28]. We assume this electron bunch is on-crest accelerated in a S-band RF structure with frequency of 2856 MHz and peak energy gain of 50 MeV. Neglecting the space-charge effect, the nonlinearity of the energy chirp is identical to the curvature of the RF field and thus the beam initial energy profile also has a cosinoidal form [see red curves in Figs. 2(c)-2(f)]. During the propagation through the plasma, the simulated beam energy spread (RMS) reductions versus the propagation distances d_p for these three plasma densities are plotted in Fig. 2(b). Clearly, after a distance of about 32.0 mm ($n_p = 2.1\times10^{13}$ cm^{-3}) [35.9 mm ($n_p = 3.1\times10^{13}$ cm^{-3}) or 26.2 mm ($n_p = 4.1\times10^{13}$ cm^{-3})], the energy spread has been reduced from the initial 60 keV to the minimum value of about 42 keV ($n_p = 2.1\times10^{13}$ cm^{-3}) [16 keV ($n_p = 3.1\times10^{13}$ cm^{-3}) or 21 keV ($n_p = 4.1\times10^{13}$ cm^{-3})]. The corresponding LPS distributions are shown in Figs. 2(c)-2(e) with blue curves and the energy spec-

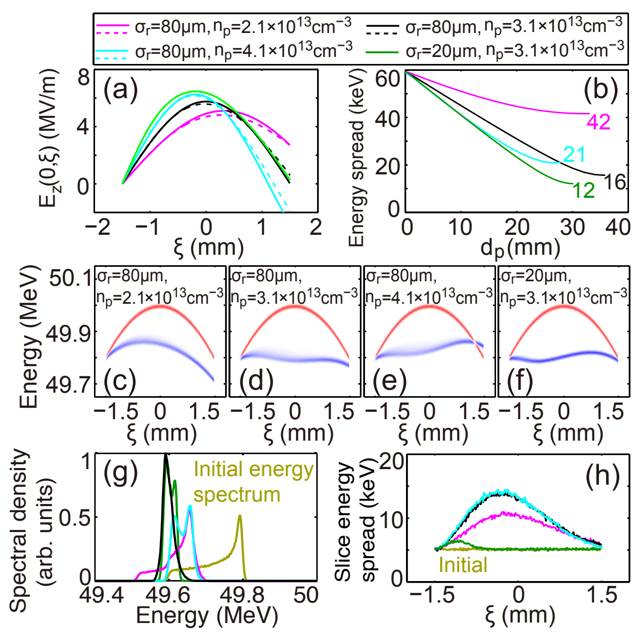

FIG. 2. (a) Lineouts of calculated (dashed lines) and simulated (solid lines) E_z field for four different n_p and σ_r cases. (b) The energy spread (RMS) reduction versus the propagations distance d_p for these four cases. (c)-(f), The corresponding LPS before (in red) and after (in blue) the plasma linearizer for the above cases. (g), The energy spectra corresponding to (c)-(f). (h), Distributions of the beam slice energy spread (RMS) for the above four cases, where the initial RMS slice energy spread is 5 keV.

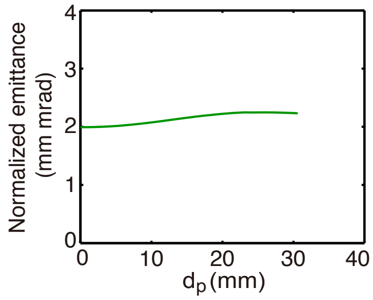

FIG. 3. The evolution of normalized emittance during the linearizing process for the case of $\sigma_r = 20$ μm and $n_p = 3.1 \times 10^{13}$ cm^{-3}.

tra are shown in Fig. 2(g). Based on above, a conclusion can be drawn that to effectively linearize the beam LPS with an ideal cosinoidal profile, E_z should also be a cosinoidal-waveform but of opposite sign (i.e., decelerating field) with a wavelength near twice the bunch length, i.e., $k_p L_b \approx \pi$. Note that, the weak dependence of E_z on r leads to small uncorrelated slice energy spread increase during the linearizing process, as shown in Fig. 2(h). Such slice energy spread growth further decreases with reducing σ_r. This may have slight or little effect on HEER and UEM performance, and might be beneficial for beam heating in FELs to partially suppress unwanted microbunching instability [29].

For an overdense beam ($n_b > n_p$), where plasma wakes evolve into the nonlinear or blowout regime, similar arguments can also be made. For instance, if we decrease σ_r in the above example to 20 μm while simultaneously keeping I_b (increasing n_b to 3.04×10^{14} cm^{-3}), n_p (3.1×10^{13} cm^{-3}) and other parameters unchanged, the simulated E_z is as shown in Fig. 2(a) with the green line. One can see that although the waveform of E_z is slightly different from that in the linear regime case, the linearizing mechanism is still effective and the final achievable minimum energy spread (12 keV with $d_p = 30.1$ mm) is even lower than that in the linear regime case [see the green line in Fig. 2(b)]. The final beam LPS is shown in Fig. 2(f) with the blue curve and the corresponding energy spectrum is shown in Fig. 2(g) with the green line. Furthermore, if $n_b \gg n_p$, the majority of the beam is located in a fully blown-out ion channel, such that E_z is constant in r, leading to slice energy spread preservation [see the green curve in Fig. 2(h)]. At the same time, the focusing wakefield is independent of ξ, and this will help to maintain the beam emittance [e.g., the normalized emittance in the above case only grows by ~10% of the initial value (2 mm mrad) during the linearizing process, as shown in Fig. 3]. This property of preserving the slice energy spread and emittance of the beam core is an advantage of linearizers over dechirpers based on uniform plasmas. In a uniform plasma dechirper, where the plasma wavelength is much larger than the bunch length, the excited wakefield within the beam is a linear plasma wake even if $n_b > n_p$. Therefore, similar to the underdense beam case, during the dechirping process, the beam slice energy spread will also increase due to r-dependent E_z and the beam emittance will also grow due to ξ-dependent focusing wakefield [22].

III. EXPERIMENTAL DEMONSTRATION

.

To confirm the above predictions, we have performed a plasma linearizing experiment at Tsinghua University [30, 31]. The schematic experimental layout is shown in Fig. 4(a). A ~10-ps (full length), 370-pC, 50-MeV electron beam with a nonlinear energy chirp is generated by a high-brightness S-band photocathode-RF-gun-driven linac. To effectively cancel the nonlinear energy chirp, in practice, a beam having a near flat-top current distribution is preferred. This is achieved by shaping the temporal distribution of the laser to a near flat-top profile through the pulse stacking technique using BBO crystals [32, 33]. The bunch charge is set by controlling the energy of the 266-nm photocathode-drive laser. The nonlinear energy chirp is imprinted by near on-crest acceleration in the accelerating structure. The electron beam is focused by two triplets to a transverse size $\sigma_r = 60.4$ μm [Fig. 4(b)] at the front edge of a slit gas jet, and detected by a removable OTR screen [Screen1 in Fig. 4(a)]. The normalized emittance is measured to be ~2 mm mrad by using a two-screen method [Screen1 and Screen2 (Ce:YAG) about 2 m downstream][34]. The beam LPS is measured on another Ce:YAG screen [Screen3 in Fig. 4(a)] by using an RF deflecting cavity (temporal resolution ~0.4 ps FWHM) and a dipole magnet, as shown in Fig. 4(c). The projected beam current profile is shown in Fig. 4(d). Here, due to the space-charge effect, the real LPS is different from an ideal cosine function. Specifically, because the longitudinal space-charge force (when the beam is at relatively low energy) pushes the electrons in the head further forward, the energy of the particles in the bunch head is increased compared to the space-charge-free case, and thus, a "kink" is formed in the bunch head. In addition, due to the slight acceleration phase offset (with respect to the on-crest phase), the beam energy reaches peak after the beam center. To match the real LPS, a linearizing wake wavelength larger than 20 ps and thus a plasma density $\lesssim 3.1 \times 10^{13}$ cm^{-3} needs to be used.

To generate a low-density plasma with $n_p \lesssim 3.1 \times 10^{13}$ cm^{-3}, a method based on laser ionization of a mixed gas (0.1% H_2 + 99.9% He) is used, where the laser intensity is chosen properly to only ionize the hydrogen atoms. The longitudinal gas profile from the slit gas jet (30 mm by 2 mm) is measured off line using shearing interferometry by a wavefront sensor [35] with Argon gas, as shown in Fig. 4(d). A 36-fs (FWHM) 800-nm laser pulse is focused to

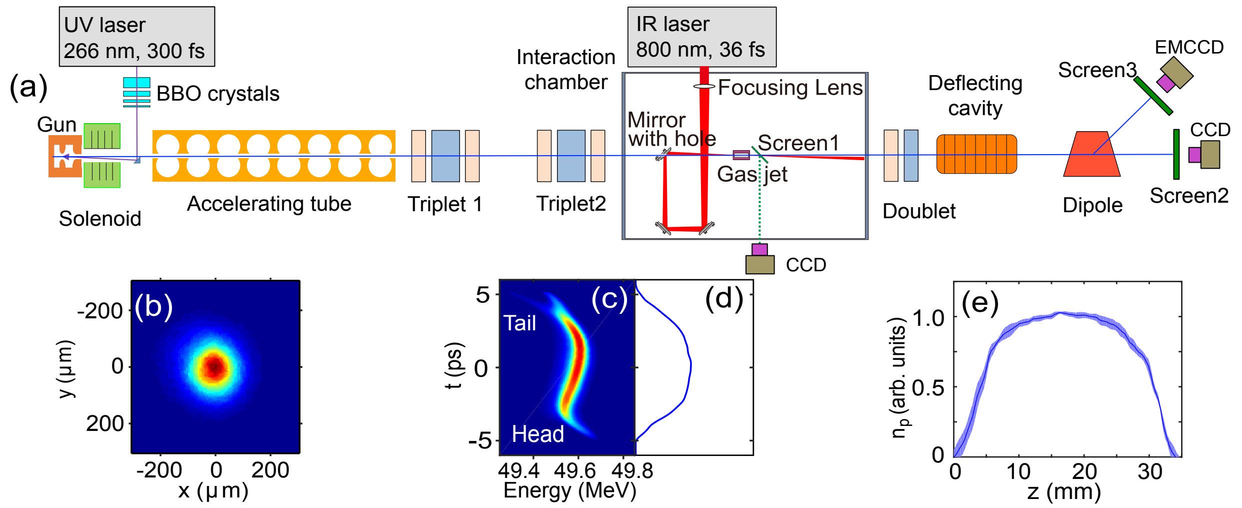

FIG. 4. (a) Schematic layout of the experiment. (b) The beam waist profile. (c) Measured LPS distribution. (d) The beam current profile. (e) Longitudinal distribution of plasma density through off-line measurement, where the shaded regions correspond to the standard deviation of 10 consecutive shots.

a waist size $w_0 \sim 110$ μm by a lens ($f = 1500$ mm) near the center of the gas jet. Right after ionization occurs, the plasma approximately has an initial radius $\sim w_0$ and a density proportional to the backing gas pressure P_g. After a proper delay (∼10 ns), the plasma expands to a wider size with a lower density. As shown in Ref. [36], the plasma expansion rate is dominated by the initial electron temperature given by the ionization, and has little dependence on the initial density. Therefore, the plasma density after expansion with given delay is approximately proportional to its initial P_g.

To demonstrate the linearizing effect with this low-density plasma, the electron beam is sent through a 3-mm central hole on the final turning mirror and focused near the front edge of the gas jet. The laser pulse collinearly propagates with and arrives about 10 ns before the electron beam with a timing jitter of ∼100 fs [37]. The electron beam has a negligible transverse position jitter at the focus (∼4 μm), and propagates through the ∼30-mm-long plasma. Figures 5(a)-5(c) show the measured LPS on Screen3 and the corresponding energy centroids (black lines) for the plasma-off case [identical to Fig. 4(c)] and plasma-on cases with two different P_g (1.0 and 1.5 MPa; similar shots under the same experimental condition can be found in Supplemental Material [38]). The energy centroids of the beam cores are fitted with a third-order polynomial, $W(t) = W_0 + \chi_1 t + \chi_2 t^2 + \chi_3 t^3$. For the plasma-off case, $\chi_2 = -5.4 \times 10^{-3}$ MeV/ps^2 and $\chi_3 = -1.5 \times 10^{-3}$ MeV/ps^3. For the plasma-on case with $P_g = 1.0$ MPa, the nonlinear energy chirp is partially reduced. For $P_g = 1.5$ MPa, the LPS is seen to be upright with the nonlinear energy chirp greatly reduced [Fig. 5(c)]. The quadratic and cubic chirp fitting parameters are abated by factors of about 5 and 10, to $\chi_2 = -1.0 \times 10^{-3}$ MeV/ps^2 and $\chi_3 = -1.4 \times 10^{-4}$ MeV/ps^3, respectively, relative to the plasma-off case. In these measurements, the horizontal size and the divergence of the beam at the entrance of the dipole limit the energy resolution to about 58 keV (FWHM), and this can be estimated directly from the expanded slice energy spread obtained by LPS measurement in Fig. 4(c), where the true slice energy spread is below 10 keV based on simulations of our beam line and measurements of similar beam lines [29, 39].

To get a deeper insight of the linearizing process, and also to alleviate the effect of the limited energy resolution, we make detailed comparisons between LPS measurements and high-fidelity 3D PIC simulations using QuickPIC. We use beam and plasma parameters in the simulations close to the experimental conditions. For the beam parameters, the measured current profile [Fig. 4(d)] and the nonlinear energy chirp deduced from the centroid of the LPS [black line in Fig. 5(a)] are used in the simulations, and the beam slice energy spread is also set to the upper limit (10 keV FWHM). For the plasma parameters, the longitudinal plasma profile is set as the measured distribution in Fig. 4(e), and the plasma density n_p is assumed to be proportional to P_g as discussed before. In Figs. 5(d)-5(f), we show the simulated LPS distributions on Screen3 and the corresponding energy centroids (dashed pink lines) obtained by scanning the single free parameter n_p to get a best fit to the experimental measurements ($n_p = 1.0 \times 10^{13}$ cm^{-3} for $P_g = 1.0$ MPa, therefore $n_p = 1.5 \times 10^{13}$ cm^{-3} for $P_g = 1.5$ MPa). Here the effect of beam transport through the downstream beam line is fully taken into account. For comparison, the energy centroids of measured LPS distributions from Figs. 5(a)-5(c) are also shown in Figs. 5(d)-5(f) with solid black lines, respectively. Clearly, the measured energy centroids agree well with the simulated ones except at the very front and rear of the bunch. In Fig. 5(j) we show a direct comparison between the measured (solid) and simulated (dotted) energy loss along the bunch. The agreement between the two is excellent for both two values of P_g. The above comparisons use only one parameter to closely match two LPS distributions, giving us confidence for the value of the plasma density used, which is too low to be directly measured on line by interferometry.

In addition to the energy centroids, we also plot the horizontal lineouts (at $t = 0$) of both the measured and simulated LPS distributions on Screen3 for the plasma-off case and the plasma-on case with $P_g = 1.5$ MPa ($n_p = 1.5 \times 10^{13}$ cm^{-3}), as shown in Fig. 6. One can clearly see that, good agreement between experiment and simulation is also obtained. This further confirms the value of the plasma density used. Both the measured and simulated FWHM spreads of the lineout increase

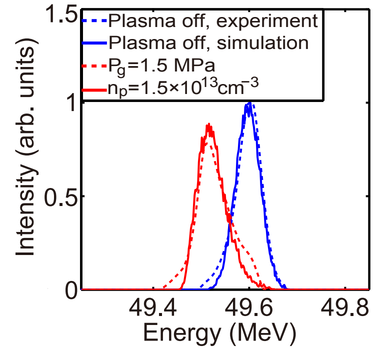

FIG. 6. The horizontal lineouts (at $t = 0$) of both the measured (dashed lines) and simulated (solid lines) LPS distributions on Screen3 for the plasma-off case and the plasma-on case with $P_g = 1.5$ MPa ($n_p = 1.5 \times 10^{13}$ cm^{-3})..

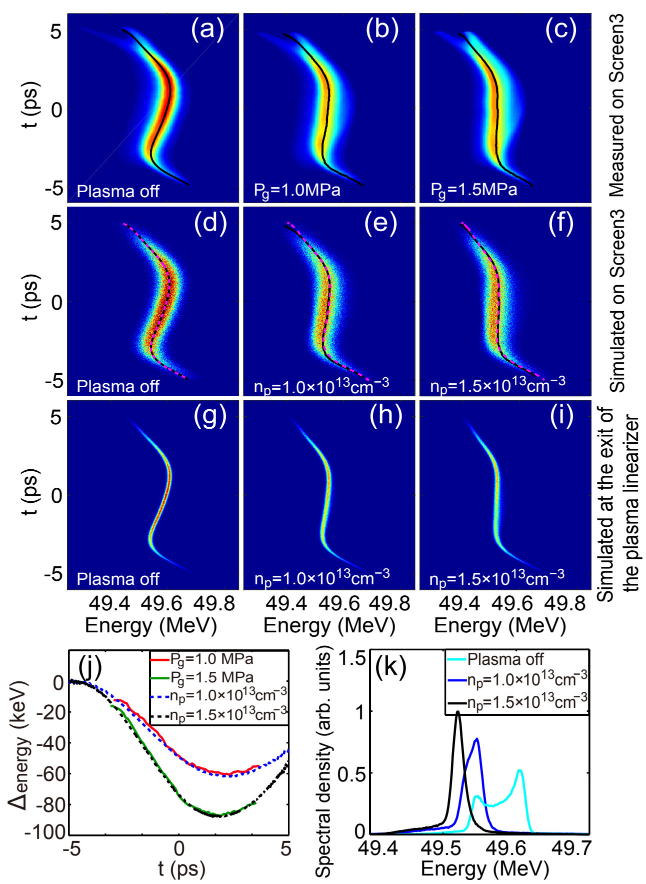

FIG. 5. (a)-(i), Beam LPS distributions [top (middle) row: the experimental (simulated) results recorded on Screen3; bottom row: the simulated results at the exit of the plasma linearizer]. The left column is for plasma-off, the middle and right columns are for plasma-on with $P_g = 1.0$ MPa ($n_p = 1.0 \times 10^{13}$ cm^{-3}) and $P_g = 1.5$ MPa ($n_p = 1.5 \times 10^{13}$ cm^{-3}), respectively. (j), Measured (solid lines) and simulated (dashed lines) results of the energy loss along the bunch. (k), The energy spectra corresponding to (g)-(i).

from ~58 keV in the plasma-off case to ~69 keV in the plasma-on case. Such growth is mainly due to two reasons. On the one hand, the intrinsic slice energy spread slightly increases during the linearizing process because of the weak dependence of E_z on the transverse dimension. On the other hand, although the beam slice emittance is approximately preserved, the beam slice divergence still increases owing to the strong plasma focusing strength, which leads to the growth of the above spread by considering the beam transport through the downstream beam line.

Based on the good agreements above, we can also get valuable information on the exact beam LPS after the plasma linearizer, which cannot be directly measured due to the limited energy resolution about 58 keV. Figures 5(g)-5(i) plot the simulated LPS distributions just at the exit of the linearizer for the cases of plasma-off, $n_p = 1.0 \times 10^{13}$ cm^{-3} and $n_p = 1.5 \times 10^{13}$ cm^{-3}, respectively. For $n_p = 1.5 \times 10^{13}$ cm^{-3}, the simulated LPS of the beam core has no obvious nonlinear feature, suggesting that at this density the nonlinear energy chirp has been removed. The total energy spread is minimum and dominated by the slice energy spread, which is much smaller than the resolution-limited measurement. The corresponding energy spectrum in Fig. 5(k) shows an energy spread of just 18 keV FWHM compared with the plasma-off case of 74 keV FWHM, leading to a near fourfold reduction in the relative energy spread (from 1.48‰ to 0.36‰).

These experimental results can be properly scaled for shorter beams used in X-band (frequency ~12 GHz) linac-based facilities. In that case, an active compensation scheme with a harmonic cavity at even higher frequency becomes difficult for lack of a suitable high-power RF source. Utilizing dielectric-lined or corrugated metallic structures requires very small geometric parameters to match the short bunch length, bringing difficulty to structure manufacturing and beam alignment. By contrast, generating a plasma with a relatively high density can be readily achieved, therefore using a plasma linearizer to remove the beam nonlinear energy spread is a highly attractive method.

In addition, although the experimental results are for relatively low-energy beams (~50 MeV), these results can still be properly scaled for high-energy beams by simply increasing the plasma length. For instance, if we change the beam energy to GeV-order and also the energy spread to MeV-order while keeping the other parameters fixed, a tens-of-centimeters-long plasma section can be used to remove the nonlinear energy chirp. A plasma section with such length may be achievable by using gas cells, capillary or alkali ovens. Moreover, we note that, a higher-energy electron beam can be typically focused to a smaller transverse size (leading to a higher beam density) than a lower-energy beam with the other parameters (charge, current, length, normalized emittance and so on) unchanged. As we addressed above, the overdense beam case is preferred for a practical linearizer application in preserving the beam emittance. Therefore, applying the linearizer to the high-energy beam case has an advantage over applying it to the low-energy beam case.

Finally, we note that for a plasma dechirper, the focus of previous papers [18–22] is on removing the linear energy chirps. While for the plasma linearizer proposed and demonstrated here, its purpose is to remove the nonlinear energy chirps. These two cases may seem similar, however, the end goal is indeed different and the physical mechanisms involved in these two regimes are obviously different. When the plasma is used as a linearizer as is the case here, in order to obtain good linearizing effect, the electron bunch current profile should be precisely shaped to be a near flat-top distribution and the plasma wavelength should be close to twice that of the bunch length. However, when the plasma is used as a dechirper as in previous papers [18–22], there is no strict limitation on both bunch current profile and plasma wavelength as long as the bunch length is much smaller than the plasma wavelength. Moreover, the plasma density in the linearizer case can be at least one to even several orders of magnitude lower than that in the dechirper case.

IV. SUMMARY

In summary, a plasma linearizing scheme that mitigates the beam nonlinear energy chirp is proposed and experimentally demonstrated. This scheme is based on the beam's self-generated quasi-cosinoidal longitudinal wake in a low-density plasma. By choosing a proper density and length, such a plasma can easily linearize a practical beam's LPS. The experimental results, combined with high-fidelity 3D PIC simulations indicate a near fourfold reduction of the nonlinear beam energy spread from 1.48‰ to 0.36‰ (FWHM). This tunable and flexible technique can be applied to numerous accelerator-based scientific facilities for significantly enhancing the beam quality.

ACKNOWLEDGMENTS

This work is supported by the National Natural Science Foundation of China (NSFC) Grants (No. 11535006, No. 11991071, No. 11775125, and No. 11875175), CAS Center for Excellence in Particle Physics, the U.S. Department of Energy Grants (No. DE-SC0010064, No. DE-SC0008491, and No. DE-SC0008316) and the U.S. National Science Foundation (NSF) Grant No. 1734315.

REFERENCES

* jfhua@tsinghua.edu.cn
† z-zhou14@tsinghua.org.cn
‡ weilu@tsinghua.edu.cn

[1] B. W. J. McNeil and N. R. Thompson, "X-ray free-electron lasers," Nature Photonics **4**, 814–821 (2010).
[2] Z. T. Zhao, D. Wang, J. H. Chen, H. X. Deng, J. G. Ding, C. Feng, Q. Gu, M. M. Huang, T. H. Lan, Y. B. Leng, et al., "First lasing of an echo-enabled harmonic generation free-electron laser," Nature Photonics **6**, 360–363 (2012).
[3] J. Amann, W. Berg, F.-J. Decker, Y. Ding, P. Emma, Y. Feng, J. Frisch, D. Fritz, J. Hastings, Z. Huang, et al., "Demonstration of self-seeding in a hard-x-ray free-electron laser," Nature Photonics **6**, 693–698 (2012).
[4] E. Allaria, D. Castronovo, P. Cinquegrana, P. Craievich, M. Dal Forno, M. B. Danailov, G. D'Auria, A. Demidovich, G. De Ninno, S. Di Mitri, et al., "Two-stage seeded soft-x-ray free-electron laser," Nature Photonics **7**, 913–918 (2013).
[5] F. E. Merrill, J. Goett, J. W. Gibbs, S. D. Imhoff, F. G. Mariam, C. L. Morris, L. P. Neukirch, J. Perry, D. Poulson, R. Simpson, et al., "Demonstration of transmission high energy electron microscopy," Applied Physics Letters **112**, 144103 (2018).
[6] Zheng Zhou, Yu Fang, Han Chen, Yipeng Wu, Yingchao Du, Lixin Yan, Chuanxiang Tang, and Wenhui Huang, "Demonstration of single-shot high-quality cascaded high-energy-electron radiography using compact imaging lenses based on permanent-magnet quadrupoles," Physical Review Applied **11**, 034068 (2019).
[7] J. Yang, M. Gohdo, K. Kan, T. Kondoh, K. Tanimura, and Y. Yoshida, "Femtosecond time-resolved transmission electron microscopy using rf gun," Proceedings of IPAC 2014, Dresden, Germany , 2205 (2014).
[8] R. K. Li and P. Musumeci, "Single-shot mev transmission electron microscopy with picosecond temporal resolution," Physical Review Applied **2**, 024003 (2014).

[9] X. Dao, F. Fu, J. Zhang, X. Huang, L. Wang, X. Wang, and W. Wan, "Accelerator-based single-shot ultrafast transmission electron microscope with picosecond temporal resolution and nanometer spatial resolution," Nuclear Instruments and Methods in Physics Research Section A: Accelerators, Spectrometers, Detectors and Associated Equipment **759**, 74–82 (2014).

[10] Paul Emma, "X-band rf harmonic compensation for linear bunch compression in the lcls," SLAC, Stanford, CA, USA, Rep. LCLS-TN-01-1 (2001).

[11] J. Arthur, W. Graves, M. Renner, J. Rosenzweig, G. Faigel, Z. Huang, M. Wulff, J. Hajdu, I. Evans, K. Kulander, et al., Linac coherent light source (LCLS) conceptual design report, Tech. Rep. (2002).

[12] G. Penco, M. Danailov, A. Demidovich, E. Allaria, G. De Ninno, S. Di Mitri, W. M. Fawley, E. Ferrari, L. Giannessi, and M. Trovo, "Experimental demonstration of electron longitudinal-phase-space linearization by shaping the photoinjector laser pulse," Physical Review Letters **112**, 044801 (2014).

[13] G. Penco, E. Allaria, I. Cudin, S. Di Mitri, D. Gauthier, S. Spampinati, M. Trovó, L. Giannessi, E. Roussel, S. Bettoni, P. Craievich, and E. Ferrari, "Passive linearization of the magnetic bunch compression using self-induced fields," Phys. Rev. Lett. **119**, 184802 (2017).

[14] P Craievich, "Passive longitudinal phase space linearizer," Physical Review Special Topics-Accelerators and Beams **13**, 034401 (2010).

[15] Haixiao Deng, Meng Zhang, Chao Feng, Tong Zhang, Xingtao Wang, Taihe Lan, Lie Feng, Wenyan Zhang, Xiaoqing Liu, Haifeng Yao, et al., "Experimental demonstration of longitudinal beam phase-space linearizer in a free-electron laser facility by corrugated structures," Physical review letters **113**, 254802 (2014).

[16] Feichao Fu, Rui Wang, Pengfei Zhu, Lingrong Zhao, Tao Jiang, Chao Lu, Shengguang Liu, Libin Shi, Lixin Yan, Haixiao Deng, et al., "Demonstration of nonlinear-energy-spread compensation in relativistic electron bunches with corrugated structures," Physical review letters **114**, 114801 (2015).

[17] A. Novokhatski, "Wakefield potentials of corrugated structures," Physical Review Special Topics-Accelerators and Beams **18**, 104402 (2015).

[18] Y. Wu, Y. Du, J. Zhang, Z. Zhou, Z. Cheng, S. Zhou, J. Hua, C. Pai, and W. Lu, "A preliminary experimental study of energy chirp reduction by a plasma dechirper," Proceedings of IPAC 2017, Copenhagen, Denmark , 1258–1260 (2017).

[19] Y. P. Wu, J. F. Hua, Z. Zhou, J. Zhang, S. Liu, B. Peng, Y. Fang, Z. Nie, X. N. Ning, C.-H. Pai, Y. C. Du, W. Lu, C. J. Zhang, W. B. Mori, and C. Joshi, "Phase space dynamics of a plasma wakefield dechirper for energy spread reduction," Phys. Rev. Lett. **122**, 204804 (2019).

[20] R. D'Arcy, S. Wesch, A. Aschikhin, S. Bohlen, C. Behrens, M. J. Garland, L. Goldberg, P. Gonzalez, A. Knetsch, V. Libov, A. Martinez de la Ossa, M. Meisel, T. J. Mehrling, P. Niknejadi, K. Poder, J.-H. Röckemann, L. Schaper, B. Schmidt, S. Schröder, C. Palmer, J.-P. Schwinkendorf, B. Sheeran, M. J. V. Streeter, G. Tauscher, V. Wacker, and J. Osterhoff, "Tunable plasma-based energy dechirper," Phys. Rev. Lett. **122**, 034801 (2019).

[21] V. Shpakov, M. P. Anania, M. Bellaveglia, A. Biagioni, F. Bisesto, F. Cardelli, M. Cesarini, E. Chiadroni, A. Cianchi, G. Costa, M. Croia, A. Del Dotto, D. Di Giovenale, M. Diomede, M. Ferrario, F. Filippi, A. Giribono, V. Lollo, M. Marongiu, V. Martinelli, A. Mostacci, L. Piersanti, G. Di Pirro, R. Pompili, S. Romeo, J. Scifo, C. Vaccarezza, F. Villa, and A. Zigler, "Longitudinal phase-space manipulation with beam-driven wakefields," Phys. Rev. Lett. **122**, 114801 (2019).

[22] Y. P. Wu, J. F. Hua, C.-H. Pai, W. An, Z. Zhou, J. Zhang, S. Liu, B. Peng, Y. Fang, S. Y. Zhou, et al., "Near-ideal dechirper for plasma-based electron and positron acceleration using a hollow channel plasma," Physical Review Applied **12**, 064011 (2019).

[23] T. Katsouleas, S. Wilks, P. Chen, J. M. Dawson, and J. J. Su, "Beam loading in plasma accelerators," Particle Accelerators **22**, 81–99 (1987).

[24] W. Lu, C. Huang, and M. M. Zhou, "Limits of linear plasma wakefield theory for electron or positron beams," Physics of Plasmas **12**, 063101 (2005).

[25] W. Lu, C. Huang, M. Zhou, W. B. Mori, and T. Katsouleas, "Nonlinear theory for relativistic plasma wakefields in the blowout regime," Phys. Rev. Lett. **96**, 165002 (2006).

[26] C. Huang, V. K. Decyk, M. Zhou, W. Lu, W. B. Mori, J. H. Cooley, T. M. Antonsen Jr., B. Feng, T. Katsouleas, and J. Vieira, "Quickpic: a highly efficient fully parallelized pic code for plasma-based acceleration," J. Phys. Confer. Series **46**, 190–199 (2006).

[27] Weiming An, Viktor K. Decyk, Warren B. Mori, and Thomas M. Antonsen Jr., "An improved iteration loop for the three dimensional quasi-static particle-in-cell algorithm: Quickpic," J. Comput. Phys. **250**, 165–177 (2013).

[28] "Quickpic open source," `https://github.com/UCLA-Plasma-Simulation-Group/QuickPIC-OpenSource`.

[29] Z. Huang, A. Brachmann, F.-J. Decker, Y. Ding, D. Dowell, P. Emma, J. Frisch, S. Gilevich, G. Hays, Ph. Hering, et al., "Measurements of the linac coherent light source laser heater and its impact on the x-ray free-electron laser performance," Phys. Rev. ST Accel. Beams **13**, 020703 (2010).

[30] Yingchao Du, Lixin Yan, Jianfei Hua, Qiang Du, Zhen Zhang, Renkai Li, Houjun Qian, Wenhui Huang, Huabi Chen, and Chuanxiang Tang, "Generation of first hard x-ray pulse at tsinghua thomson scattering x-ray source," Review of Scientific Instruments **84**, 053301 (2013).

[31] J.-F. Hua, L.-X. Yan, C.-H. Pai, C.-J. Zhang, F. Li, Y. Wan, Y.-P. Wu, X.-L. Xu, Y.-C. Du, W.-H. Huang, et al., "Generating 10-40 mev high quality monoenergetic electron beams using a 5 tw 60 fs laser at tsinghua university," Chinese Physics C **29**, 017001 (2015).

[32] L. Zheng, Y. Du, Z. Zhang, H. Qian, L. Yan, J. Shi, Z. Zhang, Z. Zhou, X. Wu, X. Su, et al., "Development of s-band photocathode rf guns at tsinghua university," Nuclear Instruments and Methods in Physics Research A **834**, 98 (2016).

[33] John G. Power and Chunguang Jing, "Temporal laser pulse shaping for rf photocathode guns: The cheap and easy way using uv birefringent crystals," in AIP Conference Proceedings, Vol. 1086 (AIP, 2009) pp. 689–694.

[34] L. Y. Zhang and J. J. Zhuang, "Calculation of two-screen emittance measurement," Nuclear Instruments and Methods in Physics Research Section A: Accelerators, Spectrometers, Detectors and Associated Equipment **407**, 356–358 (1998).

[35] J.-C. Chanteloup, "Multiple-wave lateral shearing interferometry for wave-front sensing," Applied Optics **44**, 1559–1571 (2005).

[36] N. Lemos, T. Grismayer, L. Cardoso, G. Figueira, R. Issac, D. A. Jaroszynski, and J. M. Dias, "Plasma expansion into a waveguide created by a linearly polarized femtosecond laser pulse," Physics of Plasmas **20**, 063102 (2013).

[37] Z. Lin, Y. Du, J. Yang, Y. Xu, L. Yan, W. Huang, C. Tang, G. Huang, Q. Du, L. Doolittle, et al., "Development of sub-100 femtosecond timing and synchronization system," Review of Scientific Instruments **89**, 014701 (2018).

[38] See Supplemental Material at URL for more experimental data.

[39] C. Feng, T. Zhang, J. Chen, H. Deng, M. Zhang, X. Wang, B. Liu, T. Lan, D. Wang, and Z. Zhao, "Measurement of the average local energy spread of electron beam via coherent harmonic generation," Phys. Rev. ST Accel. Beams **14**, 090701 (2011).